
[View Journal Online](#)
[View Article Online](#)

N'-(Pyridin-3-ylmethylene)benzenesulfonylhydrazide: Crystal structure, DFT, Hirshfeld surface and in silico anticancer studies

Ifeyinwa Stella Ozochukwu ¹, Obinna Chibueze Okpareke ¹, David Chukwuma Izuogu ¹, Akachukwu Ibezim ², Oguejiofo Theophilus Ujam ¹ and Jonnie Niyi Asegbeloyin ^{1,*}

¹ Department of Pure and Industrial Chemistry, University of Nigeria, Nsukka 410001, Enugu State, Nigeria
 ifystella47@yahoo.com (I.S.O.), obinna.okpareke@unn.edu.ng (O.C.O.), david.izuogu@unn.edu.ng (D.C.I.), oguejiofo.ujam@unn.edu.ng (O.T.U.), niyi.asegbeloyin@unn.edu.ng (J.N.A.)

² Department of Pharmaceutical and Medicinal Chemistry, University of Nigeria, Nsukka 410001, Enugu State, Nigeria
 akachukwu.ibezi@unn.edu.ng (A.I.)

* Corresponding author at: Department of Pure and Industrial Chemistry, University of Nigeria, Nsukka 410001, Enugu State, Nigeria.
 e-mail: niyi.asegbeloyin@unn.edu.ng (J.N. Asegbeloyin).

RESEARCH ARTICLE

ABSTRACT



doi 10.5155/eurjchem.12.3.256-264.2102

Received: 31 January 2021

Received in revised form: 01 April 2021

Accepted: 20 April 2021

Published online: 30 September 2021

Printed: 30 September 2021

KEYWORDS

Schiff base
 Crystal structure
 Hirshfeld surface
 Carboxaldehyde
 Anticancer activity
 Benzenesulfonylhydrazide

A new Schiff base, *N*'-(pyridin-3-ylmethylene)benzenesulfonylhydrazide, was synthesized and characterized by elemental analysis, IR, Mass, ¹H NMR and ¹³C NMR spectroscopy, and single-crystal X-ray determination. The asymmetric molecule crystallized in the monoclinic crystal system and *P*2(1)/*c* space group. Crystal data for C₁₂H₁₁N₃O₂S: *a* = 9.7547(4) Å, *b* = 9.8108(4) Å, *c* = 13.1130(5) Å, β = 109.038(2)°, *V* = 1186.29(8) Å³, *Z* = 4, μ(MoKα) = 0.270 mm⁻¹, *D*_{calc} = 1.463 g/cm³, 13338 reflections measured (5.296° ≤ 2θ ≤ 55.484°), 2790 unique (*R*_{int} = 0.0494, *R*_{sigma} = 0.0400) which were used in all calculations. The final *R*₁ was 0.0345 (*I* > 2σ(*I*)) and *wR*₂ was 0.0914 (all data). In the crystal structure of the compound C₁₂H₁₁N₃O₂S, molecules are linked in a continuous chain by intermolecular of N⋯HN=N hydrogen bonds. The pyridine moiety is planar, while the benzenesulfonylhydrazide group adopts a *gauche* conformation about C-S-N angle (105.54°). The Hirshfeld surface analysis and fingerprint plots were used to establish the presence, nature, and percentage contribution of the different intermolecular interactions, including N-H⋯N, C-H⋯O, C-H⋯C, and π⋯π interactions, with the C-H contacts having the most significant contribution. The pairwise interaction energies were calculated at the B3LYP/6-31G(d,p) level of theory, and interaction energy profiles showed that the electrostatic forces had the most significant contribution to the total interaction energies of the different molecular pairs in the crystal. *In-silico* technique was used to examine the compound as a possible anticancer agent. The molecule demonstrated zero violation of the criteria of Lipinski's rule of five with a polar surface area of 116.03 Å². The molecule displayed favorable binding interactions with ten selected validated anticancer protein targets ranging from -9.58 to -11.95 kcal/mol and -2.73 to -5.73 kcal/mol on scoring and rescoring, respectively, with London dG and Affinity dG scoring functions. Two proteins; farnesyl transferase and signaling protein, preferred interactions with the Schiff-base over their co-crystallized inhibitors according to London dG scoring. Analysis of binding poses indicated that the Schiff-base made contact with amino acid residues of the two proteins through the N-H, sulphonyl oxygen, and phenyl groups, and this could be exploited in chemical and structural modification towards activity optimization.

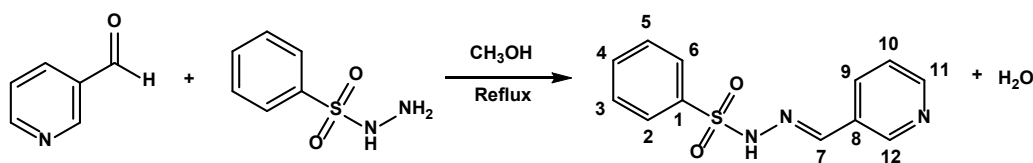
Cite this: *Eur. J. Chem.* 2021, 12(3), 256-264

Journal website: www.eurjchem.com

1. Introduction

N-Heterocyclic Schiff bases and their metal complexes have received considerable attention from researchers for decades because of their exciting coordination chemistry, pharmaceutical importance, and high biological activity [1-4]. Many Schiff base compounds have been reported to show high response when tested for *in vitro* and *in vivo* biological activities [5-7]. The wide range of pharmacological profiles exhibited by Schiff bases includes anticancer activity [6,8-12], anticonvulsant [13], analgesic, and anti-inflammatory activities [14]. Cancer is caused by an abnormal and uncoordinated growth of

a mass of tissue, which continues to multiply after cessation of the stimuli which initiated it [15]. About 7.6 million death amounting to about 13% of all death is caused by cancer per year, and this makes it the second most common disease-related cause of death within the human population [16]. There are reports of rise in cancer cases in spite of all efforts to cope with the menace [17]. Therapeutic options for cancer include the use of radiation, surgery, and drugs [18]. For decades, platinum metal-based drugs have been used for cancer treatment, however, some side effects among which include nephrotoxicity, neurotoxicity, ototoxicity, nausea and vomiting, coupled with observed resistance developed to some of the drugs



Scheme 1. Preparation of *N'*-(pyridin-3-ylmethylene)benzenesulfonylhydrazide (PMB).

have limited their clinical applications [19-21]. Researchers have continued to search and develop alternative metal-based and nonmetal-based drugs to improve the potential and the effectiveness against cancer. The title compound, *N'*-(pyridin-3-ylmethylene)benzene sulfonylhydrazide is a new Schiff base; herein is reported, its crystal structure and overall conformation. The ability of the molecule to interact with validated receptors targeted for cancer treatment using docking methods is also reported. Furthermore, the Hirshfeld surface analysis and fingerprint plots were used to establish the presence, nature, and percentage contribution of the different types of intermolecular interactions in the crystal.

2. Experimental

2.1 Materials and physical methods

Benzene sulfonylhydrazide and 3-pyridinecarboxaldehyde were used as obtained from Fluka without further purification. All other chemical substances used were reagent grade commercial products. ^1H NMR and ^{13}C NMR spectra were acquired on a Bruker 400 MHz spectrometer, using CDCl_3 as the solvent. Mass spectra were acquired using a Bruker MicrOTOF ESI-MS spectrometer. Fourier Transform Infrared (FTIR) spectra were recorded in the range of 4000-400 cm^{-1} as KBr discs on a Perkin Elmer 100 Infrared Spectrophotometer. Melting point ranges were obtained with a Fisher John melting point apparatus. Elemental analyses of C, H and N were performed using a Carlo Erba Elemental analyzer EA1108. The X-ray crystallographic data were obtained at the University of Auckland on a Bruker SMART APEX II diffractometer.

2.2. Synthesis of *N'*-(pyridin-3-ylmethylene)benzene sulfonylhydrazide (PMB)

The title compound, *N'*-(pyridin-3-ylmethylene)benzene sulfonylhydrazide, was synthesized as follows: A solution of 3-pyridinecarboxaldehyde (107 mg, 1 mmol) in methanol 10 mL was mixed with a solution of benzene sulfonylhydrazide (172 mg, 1 mmol) in methanol, 10 mL. The mixture was refluxed for 3 h, and the resulting solution was cooled to obtain whitish product which was filtered, dried, and recrystallized in methanol (Scheme 1). Crystals suitable for X-ray crystallographic analysis were obtained by slow evaporation of a methanolic solution of the compound at room temperature for 24 h. Color: Colorless. Yield: 89 %. M.p.: 160-162 °C. FT-IR (KBr, ν , cm^{-1}): 3439 (N-H), 1606 (C=N), 1120 (N-N). ^1H NMR (400 MHz, CDCl_3 , δ , ppm): 8.7 (s, 1H, N-H), 8.5 (s, 1H, HC=N), 8.0-7.8 (m, 5H, Ph), 7.4-7.2 (m, 4H, Py). ^{13}C NMR (100 MHz, CDCl_3 , δ , ppm): 133.63 C1, 129.64 C2, 127.64 C3, 124.41 C4, 127.64 C5, 129.64 C6, 151.20 C7, 139.28 C8, 129.10 C9, 133.73 C10, 144.94 C11, 148.82 C12. ESI-MS (m/z) calcd. $[\text{M}+\text{Na}]^+$ 284.29, found: $[\text{M}+\text{Na}]^+$ 284.05; calcd. $[\text{M}+\text{H}]^+$ 262.31, found $[\text{M}+\text{H}]^+$ 262.07. Anal. calcd. for $\text{C}_{12}\text{H}_{11}\text{N}_3\text{O}_2\text{S}$: C, 55.16; H, 4.24; N, 16.08. Found: C, 55.46; H, 3.95; N, 15.90 %.

2.3. Crystal structure determination

An arbitrary sphere of data were collected on a colorless block-like crystal, having approximate dimensions of 0.400 ×

0.220 × 0.200 mm, on a Bruker APEX-II diffractometer using a combination of ω - and ϕ -scans of 0.5° [22]. Data were corrected for absorption and polarization effects and analyzed for space group determination. The structure was solved by direct methods and expanded routinely [23]. The model was refined by full-matrix least-squares analysis of F^2 against all reflections. All non-hydrogen atoms were refined with anisotropic thermal displacement parameters. Unless otherwise noted, hydrogen atoms were included in calculated positions. Thermal parameters for the hydrogens were tied to the isotropic thermal parameter of the atom to which they are bonded (1.5 × for methyl, 1.2 × for all others). The software SMART was used for the collection of data frames, for indexing reflections, and to determine lattice parameters; SAINT was also used for the integration of the intensity of the reflections and for scaling. SADABS was used for empirical absorption correction. The structure was solved using SHELXS-97 and SHELXL-97 was also used for structure refinement and reporting. The structure was refined by full-matrix least-squares based on F_o^2 (SHELXL-97) with anisotropic thermal parameters for non-hydrogen atoms.

2.4. Hirshfeld surface

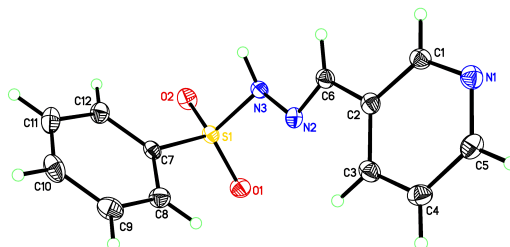
Hirshfeld surfaces (HSs) and corresponding two-dimensional fingerprint plots (FPs) were calculated using the Crystal Explorer Software 17.5 [24]. The crystallographic information files (CIF) obtained from the single-crystal X-ray measurements were used for the HS analysis. The Hirshfeld surfaces mapped over d_{norm} , shape index, and curvedness were generated according to described procedures [25,26], and used for further analysis of the intermolecular interactions in the crystal structure.

2.5. In-silico anticancer study

The builder interface implemented in the molecular operating environment (MOE) [27] software was used to generate the three-dimensional chemical structure of the Schiff base energy minimized to a gradient of 0.001 kcal/mol and saved in mol2 format. The following parameters were computed: molar weight (MW), number of rotatable bonds (NRB), hydrogen bond acceptor/donor (HBA/HBD), and lipophilicity ($\log P$), using the molecular descriptor calculator included in the QuSAR module of MOE software. The X-ray crystal structures of all ten protein-targets co-crystallized with their inhibitors were retrieved from the protein databank (PDB codes: 1GS4, 2X9E, 2XMY, 3E37, 3EP2, 3KKP, 3PP1, 4ACM, 4BBG, and 4M8H). The target-ligand complexes were treated according to standard for docking purposes, and the dock protocols were validated following the root mean square deviation (RMSD) method [28]. The dock protocols, which gave conformation of the docked ligands within ≤ 2.00 Å from that of the X-ray crystallized ones were retained and used in docking the Schiff-base into the protein binding sites. The produce receptor-ligand complexes were, respectively, scored and rescored by London dG and Affinity dG scoring methods implemented in the MOE package.

Table 1. Crystal data and structure refinement details for **PMB**.

Empirical formula	C ₁₂ H ₁₁ N ₃ O ₂ S
Formula weight	261.30
Temperature (K)	172(2)
Crystal system	Monoclinic
Space group	<i>P2₁/c</i>
a (Å)	9.7547(4)
b (Å)	9.8108(4)
c (Å)	13.1130(5)
α (°)	90
β (°)	109.038(2)
γ (°)	90
Volume (Å ³)	1186.29(8)
Z	4
ρ _{calc} (g/cm ³)	1.463
μ (mm ⁻¹)	0.270
F(000)	544.0
Crystal size (mm ³)	0.400 × 0.220 × 0.200
Radiation	MoKα (λ = 0.71073)
2θ range for data collection (°)	5.296 to 55.484
Index ranges	-12 ≤ h ≤ 12, -12 ≤ k ≤ 12, -17 ≤ l ≤ 17
Reflections collected	13338
Independent reflections	2790 [R _{int} = 0.0494, R _{sigma} = 0.0400]
Data/restraints/parameters	2790/0/167
Goodness-of-fit on F ²	1.060
Final R indexes [I ≥ 2σ (I)]	R ₁ = 0.0345, wR ₂ = 0.0872
Final R indexes [all data]	R ₁ = 0.0411, wR ₂ = 0.0914
Largest diff. peak/hole (e.Å ⁻³)	0.37/-0.41

**Figure 1.** Molecular structure of **PMB** and atoms numbering scheme at 50% probability level for non-H atoms.

3. Results and discussion

3.1. Spectroscopic studies

The FTIR spectra of **PMB** exhibit a strong broad peak at 3439 cm⁻¹, which is ascribed to the intermolecular hydrogen-bonded N-H stretching vibration of the hydrazone moiety. The imine ν(C=N) vibration appeared at 1606 cm⁻¹, similar to frequencies observed in related compounds [29,30]. The characteristic C-H stretches of aromatic groups were found at 3018 cm⁻¹, and ν(N-N) was observed at 1120 cm⁻¹. In the ¹H NMR spectra the N-H proton was found at relatively high frequency of δ 8.7 ppm corresponding to a hydrogen-bonded proton. The azomethine proton was also deshielded, and observed at δ 8.5 ppm [5]. The multiplet peak at δ 7.8-8.0 ppm was assigned to the five protons of the phenyl moiety, while the peak at δ 7.2-7.4 ppm was assigned to the pyridinyl protons. The ¹³C NMR spectra showed ten carbon signals, and these correspond to the molecular formula of **PMB**. The peak at δ 151.20 ppm was assigned to the (-C=N-) carbon; other assignments are as presented in Section 2.2. The ESI mass spectra of **PMB** showed molecular ions of [M+Na]⁺ at *m/z* 284.05. The [M+H]⁺ ion is also visible at *m/z* 262.068.

3.2. Crystal structure description of **PMB**

The molecular structure of **PMB** with the atom numbering scheme is shown in Figure 1. The compound crystallized as colorless block-like crystals. There are four molecules of the Schiff base in the unit cell of the primitive centrosymmetric monoclinic crystal system, with a space group *P2₁(1)/c*. The bond length of C6-N2 is 1.2814(21) Å, indicating the existence

of imine C=N in the compound. In the crystal structure, the molecules of the Schiff base C₁₂H₁₁N₃O₂S, are linked in a continuous chain by an intermolecular hydrogen bond from N3 to N1 of the pyridyl moiety related by the 2₁-screw axis (Figure 2). This results in a one-dimensional helical chain of H-bond molecules parallel to the *b*-axis. The pyridine moiety is planar, while the benzenesulfonylhydrazone group adopts a *gauche* conformation about C-S-N angle (105.54°). Bond distance and angles within the molecule are as expected. The crystal data and structure refinement details, selected bond lengths and angles, and intramolecular hydrogen bond distances of **PMB** are summarized in Tables 1-3, respectively. The bond length of N2-C6 (1.281 Å) suggests a double bond character as previously reported for similar compounds [4,31]. The hydrazine N2-N3 bond length of 1.399 Å, shows somewhat double bond characteristics, due to the conjugation between the π electrons on the azomethine group and lone pairs of electrons on N3 [5]. The higher bond length of S1-O2 (1.435 Å) compared to S1-O1 (1.400 Å) can be ascribed to the noncovalent bond interaction between the electronegative oxygen O2-S1 and hydrogen H-C6, which are in closer proximity. The N2-N3 nitrogen atoms adopted the more stable trans-conformation to minimize the steric strain of the substituents. The bond lengths of the pyridine group are all indicative of an aromatic system. However, the bond angle of N1-C1-C2 of 123.40° is higher than expected for *sp*² hybridized carbon of 120° because of the conjugation of the nitrogen lone pairs with the π electrons of the aromatic system. The sulphonyl group adopted a distorted tetrahedral geometry, as can be seen from the O1-S1-O2 and O2-S1-N3 bond angles of 120.87 and 104.12°, respectively. This is because of the lone pair of electrons on the sulfur atom as it adopts *dsp*³ hybridization.

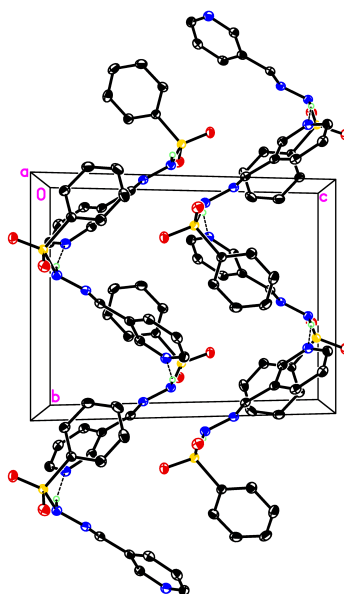
Table 2. Selected bond lengths (Å) and bond angles (°) for PMB.

Bond lengths (Å)			
O(1)-S(1)	1.4300(11)	N(3)-H(3N)	0.92(2)
O(2)-S(1)	1.4346(11)	N(3)-S(1)	1.6524(12)
C(1)-N(1)	1.3452(19)	N(2)-N(3)	1.3987(17)
C(1)-C(5)	1.338(2)	C(7)-S(1)	1.7636(14)
C(1)-H(1)	0.9300	C(6)-N(2)	1.2814(19)
C(2)-N(1)	1.3452(19)	C(2)-C(3)	1.398(2)
Bond angles (°)			
N(1)-C(5)-C(4)	123.17(14)	N(1)-C(1)-C(2)	123.40(13)
N(1)-C(5)-H(5)	118.4	N(1)-C(1)-H(1)	118.3
N(2)-N(2)-C(6)	114.74(12)	O(1)-S(1)-O(2)	120.87(7)
O(2)-S(1)-N(3)	104.12(6)	O(1)-S(1)-N(3)	107.76(6)
N(2)-C(6)-C(2)	119.95(13)	N(2)-N(3)-H(3N)	115.0(13)
N(2)-N(3)-S(1)	113.86(9)	N(3)-S(1)-C(7)	105.55(6)

Table 3. Intramolecular hydrogen bond for PMB.

D-H...A	d(D-H), Å	d(H...A), Å	d(D...A), Å	∠(DHA), °
N(3)-H(3N)...N(1)#1	0.92(2)	2.00(2)	2.8964(18)	166.3(19)

Symmetry transformation used to generate equivalent atoms: #1-x+1, y-1/2, -z+1/2.

**Figure 2.** The packing diagram of PMB shows intermolecular N...H-N hydrogen bonds as dotted lines.

3.3. Hirshfeld surface analysis

The Hirshfeld surface of PMB mapped over the d_{norm} shows the most intense red regions around the N-H groups resulting from the azomethine-N3-H3...N1 (pyridyl) intermolecular hydrogen bonding interactions (Figure 3a). Apart from the intense red spots from N-H intermolecular contacts, there are a number of other weak intermolecular contacts resulting in the rest of the d_{norm} surface having white to blue gradient coloration. Some of these contacts include phenyl- π ... π (pyridyl) interactions depicted as red dotted lines in Figure 3b resulting from C1...C12 and C5...C11 intermolecular contacts. Other intermolecular contacts are the azomethine N-H... π (pyridyl) in red and phenyl-C-H...O (sulphonyl) shown as purple lines in Figure 3c and the phenyl-C-H...S (sulphonyl) interactions (Figure 3d). The C-H... π interactions in PMB can also be analyzed by mapping the Hirshfeld surface over the shape index and curvedness surfaces (Figure 4). The donors and acceptors of intermolecular C-H... π contacts are recognized as blue and red regions around the participating atoms [25,26]. The C...H/H...C contacts in a molecule are responsible for the molecular packing in the supramolecular structure and depict the C-H... π interactions [33]. These interactions appear as hollow orange areas (π ...H-C) and bulging blue areas (C-H... π) in the compound. The small blue regions surrounding a bright

orange spot within the phenyl ring of the PMB molecule are an indication of π ... π stacking. In addition, the C4-H4...C8 and C8-H8...C4 contacts in pink-colored dotted lines in the shape index mapped isosurface in the molecule (Figure 4a) are typical examples of π ... π interactions. Further, the flat regions around the phenyl and pyridyl rings on the Hirshfeld surface mapped over curvedness in Figure 4b is another testament to the presence of π ... π interactions in the molecule.

3.3.1. Finger print plots

The 2-D Finger print plots illustrate the overall and percentage contributions of the intermolecular contacts in the molecule [32,33]. The overall fingerprint plot for PMB and those delineated into H...N/N...H, H...C/C...H, H...H, H...O/O...H, and C...O/O...C are illustrated in Figure 5a-f, and their percentage contributions are presented in Table 5. The overall fingerprint plot comprises all intermolecular contacts in the molecule, and this exhibits a shield-like profile with two symmetric spikes on each side of a triangular protrusion (Figure 5a). These spikes are also observed in the fingerprint plots for the N...H/H...N contacts in Figure 5b but not in the other surface contacts in Figures 5c-e. This is a clear indication that these spikes are representative of the N3-H3...N1 hydrogen bonding interaction in the crystal structure of the

Table 5. Percentage contribution to intermolecular contacts on the Hirshfeld surface calculated for PMB.

Contact	Percentage contribution (%)
H...N/N...H	15.6
H...C/C...H	26.3
H...H	29.9
H...O/O...H	23.1
C...O/O...C	3.1
C...C	2.0

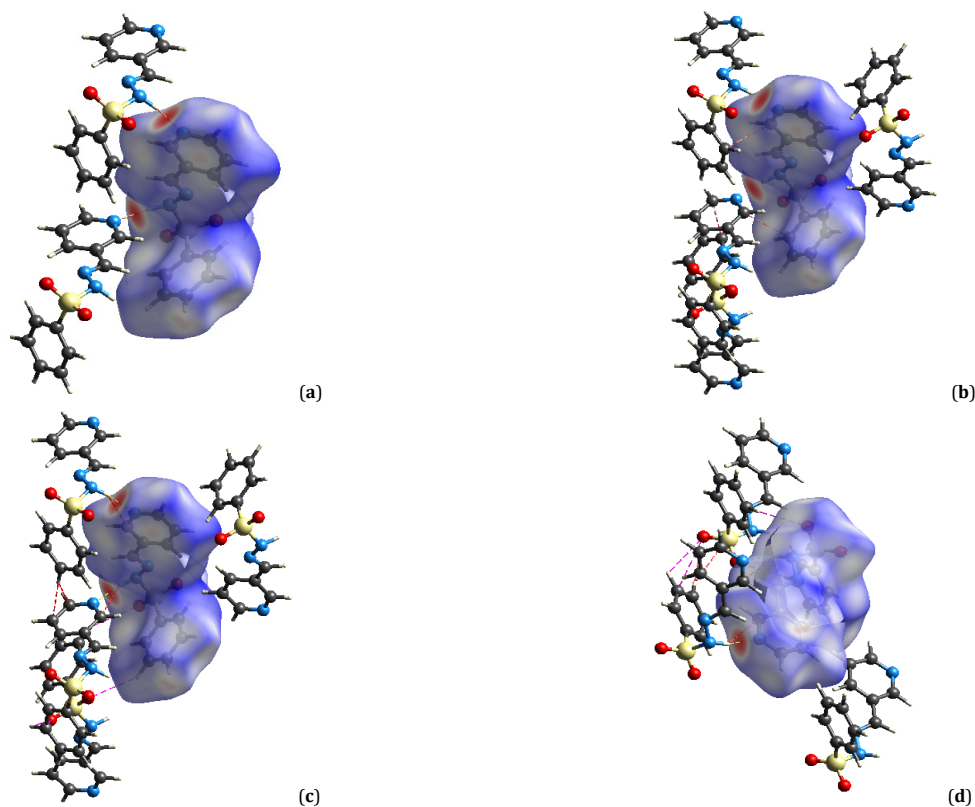


Figure 3. Hirshfeld Surface interactions mapped over d-norm show (a) the main dark red spots on the molecule showing azomethine-N-H...N (pyridyl) hydrogen bonding interactions, (b) Phenyl- π ... π (pyridyl), (c) azomethine N-H... π (pyridyl) in red and phenyl-C-H...O (sulphonyl) in purple lines, (d) phenyl- π ...O (sulphonyl) and phenyl-C-H...S (sulphonyl) purple lines.

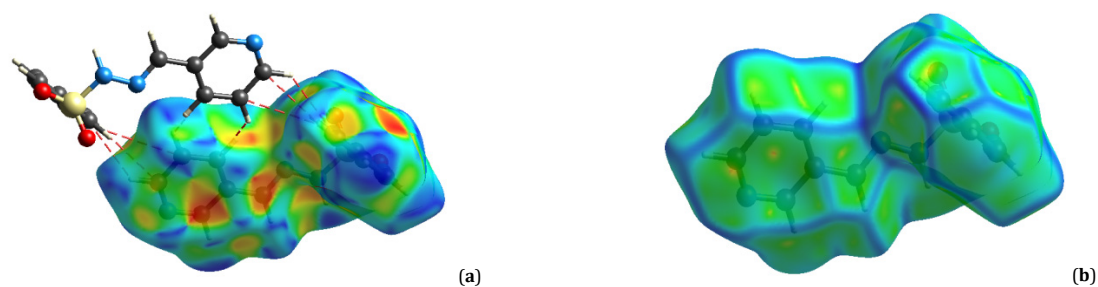


Figure 4. The Isosurface representation mapped over the shape index and curvedness isosurfaces.

compound and contributes about 15.6% to the overall intermolecular surface contacts in the molecule. The other major surface contacts in the molecule are the C...H/H...C (26.2%), H...H (29.9%), H...O/O...H (23.0%), and C...O/O...C (3.0%), showing that C1-H1...O2 intermolecular interactions contribute a combined total of 56.1 % to the overall surface contact in the molecule making it the most significant set of interactions in the crystal lattice. The fingerprint plots also show uneven distribution between the internal (i.e., the donor or acceptor atoms internal to the surface) and the external (i.e., the donor or acceptor atoms external to the surface). The H...N/N...H, H...O/O...H and C...O/O...C contacts are all inclined towards the (internal)-N...H (external) 8.7%, (internal) O...H

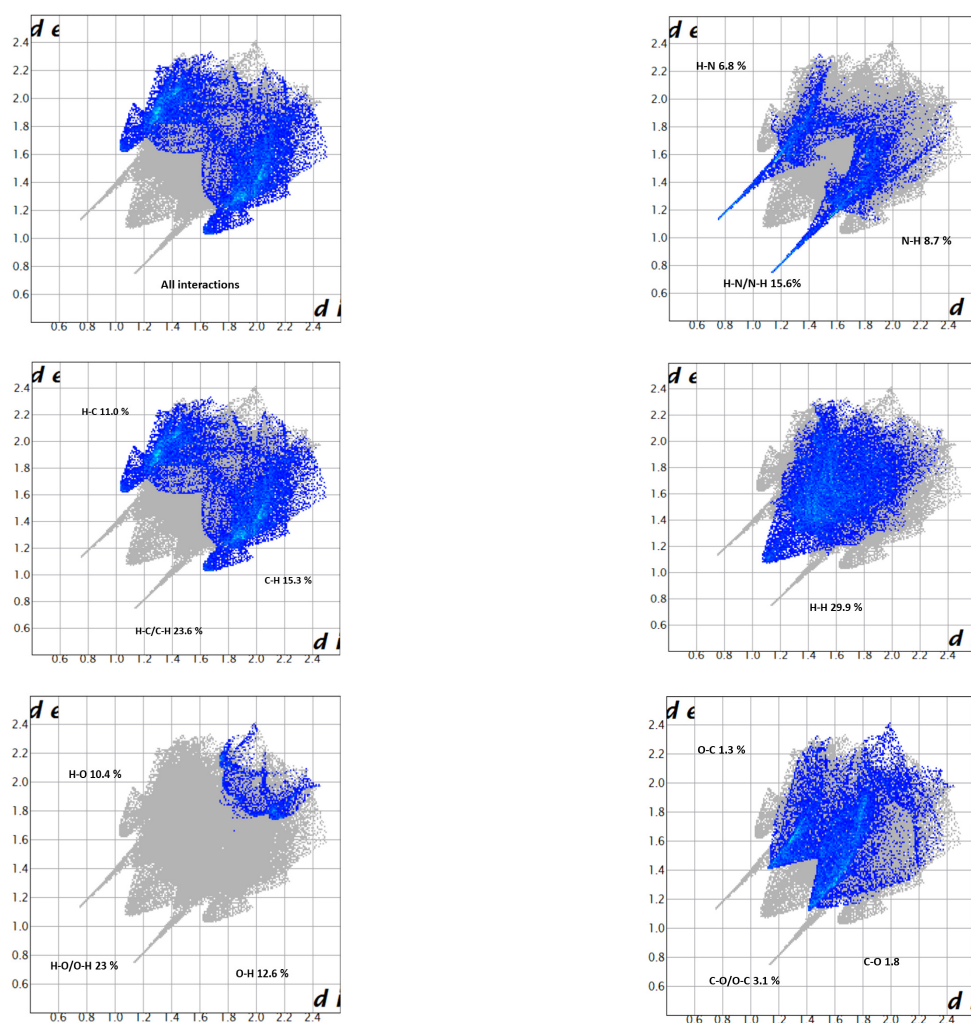
(external) 12.6%, (internal) C...O (external) 1.8% and (internal) C...H (external) with a slightly higher inclination at 15.3%. These results are slightly different from the distributions reported for *N,N*-bis-(pyridine-4-ylmethyl) ethane diamine [32].

3.3.2. Interaction energy calculations

The interaction energies between pairs of molecules within the crystal of PMB were calculated by adding up the four energy components comprising of the electrostatic (E_{ele}), polarization (E_{pol}), dispersion (E_{dis}), and exchange repulsion (E_{rep}) [24].

Table 6. A summary of the calculated interaction energies for PMB (kJ/mol).

Contact	Symmetry	R	E_{ele}	E_{pot}	E_{dis}	E_{rep}	E_{tot}
O2-H6	$x, -y+1/2, z+1/2$	7.00	-11.5	-3.9	-29.5	19.5	-28.7
C5-H11	$-x, -y, -z$	9.32	-6.5	-2.3	-14.1	9.3	-15.1
H12-H12	x, y, z	9.81	-1.8	-1.0	-17.7	14.3	-9.2
N1-N3	$-x, -y, -z$	6.21	-36.2	-8.5	-30.3	34.4	-49.7
H9-O1	$x, -y+1/2, z+1/2$	9.85	-2.5	-1.8	-11.4	5.2	-10.6
C3H3-N	$-x, y+1/2, -z+1/2$	7.17	-52.7	-13.2	-31.5	71.1	-49.0
O2-H1	$-x, y+1/2, -z+1/2$	6.91	-16.1	-5.3	-26.8	17.9	-33.3
H10-C4	$-x, -y, -z$	10.81	2.7	-0.3	-1.7	0.0	1.2
O2-H6	$-x, -y, -z$	8.76	8.6	-1.0	-1.9	0.0	6.7
C4-C10	$-x, -y, -z$	8.28	2.5	-1.8	-21.6	12.8	-9.5

**Figure 5.** 2-Dimensional Fingerprint plot of the main intermolecular interactions and contacts in the crystal structure of PMB.

The energies were obtained by calculating the wave function of each pair of molecules or atoms at the B3LYP/6-31G(d,p) level of theory [34]. Quantitative estimations of the strength and nature of the intermolecular interactions in PMB crystal with individual energy components (E_{ele} , E_{pot} , E_{dis} , and E_{rep}) as well as the sum of the energy components E_{tot} are presented in Table 6. The table shows that the electrostatic and dispersive components make the most significant contribution to the total interaction energy profile in the crystal structure. The N3-H3-N hydrogen bonding interaction between the azomethine and pyridyl ring has the most significant total interaction energies. The O2-H6, O2-H1, and O1-H9 short contacts from the intermolecular C-H...O interactions are the next in line with considerable interaction energies. The C-H and C-C and H-H contacts are at the bottom of the energy ladder compared to the other interactions in the crystal lattice. A

graphical representation of the magnitude of the interaction energies is presented in Figure 6a-d in the form of an energy framework to show the crystal supramolecular architecture using cylindrical poles joining the centroids of molecular pairs. The red, green, and blue color-coded frameworks in 6a, 6b, and 6c respectively, represent E_{ele} , E_{dis} , and E_{tot} energy components for intermolecular interactions in PMB crystal, while 6d is the annotated E_{tot} energy. The magnitude of the cylindrical pipes indicates the significance of the E_{ele} energy component to the total interaction energy and molecular packing in the crystal.

3.4. In-silico anticancer studies

PMB was investigated for its ability to bind to ten validated selected anticancer drug targets. To determine its pharmacokinetic profile as a potential drug candidate, the Lipinski rule

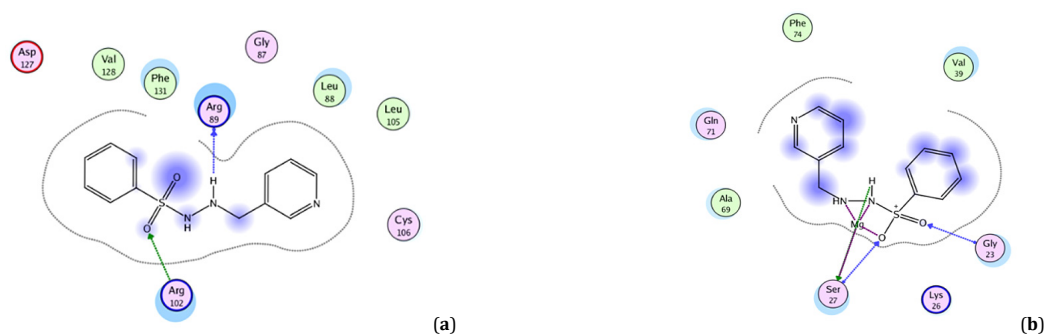


Figure 7. Binding poses of PMB towards (a) protein farnesyltransferase and (b) signaling protein binding sites.

and signaling protein higher than their co-crystallized ligands whereas Affinity dG ranked all co-crystallized ligands higher than PMB. The interesting binding affinities demonstrated by PMB suggest that it could inhibit those enzymes *in vitro* and possibly prove poisonous to cancerous cells in a biological assay. The molecule could be developed into either farnesyl transferase or signaling protein inhibitor because it outperformed known inhibitors of the two enzymes, which are greatly importance in cancer [36,37]. Close examination of the molecule's binding modes to both metalloenzymes (farnesyl transferase and signaling protein) revealed that it bound through its NH sulphonyl oxygen atom and phenyl group. Hydrogen bonds between the sulphonyl oxygen atom and Arg102, NH and Arg89 and the π - π contact between phenyl group and Phe131 could account for the significant interaction of PMB with farnesyl transferase (Figure 7a). Docking calculation by MOE DockTool identified the unique binding pose of PMB in the signaling active protein cavity. Unlike in farnesyl transferase, the magnesium atom at the binding site of the protein was found to make active contribution in the binding interaction of PMB with signaling protein (Figure 7b) and this should be exploited in the chemical structural modification process towards activity optimization. It is noteworthy that the functional units of the compound played a significant role in binding relationship with the amino acid residues at the active site of the metalloenzymes.

4. Conclusion

A Schiff base; *N*'-(pyridin-3-ylmethylene)benzenesulfonylhydrazide, was synthesized by reacting equimolar benzene sulfonylhydrazide and 3-pyridinecarboxaldehyde. The structure of the compound was confirmed by elemental analysis, spectroscopic techniques (FT-IR, ESI-MS, ^1H and ^{13}C NMR) and X-ray crystallography. The compound crystallized in the imine form. Hirshfeld surface analysis indicated the presence of both hydrogen bonding and intermolecular π - π interactions in the supramolecular architecture of the compound, and the results of the calculated pairwise interaction energies showed that the electrostatic forces had the most significant contribution to the total interaction energy of the different molecular pairs in the crystal. *In-silico* studies revealed that the compound is drug-like, and it made favorable binding interactions with ten selected anticancer drug targets. Moreover, since it showed greater binding affinity for farnesyltransferase and signaling proteins than their co-crystallized ligands and exhibited unique binding interactions with the metalloenzymes' binding site residues, it merits further attention to develop it into their efficient inhibitors and possibly anticancer agent.

Acknowledgments

We thank Dr. Tania Groutso (University of Auckland) for collection of the X-ray data sets, the University of Nigeria,

Nsukka for infrastructural support. Dr. Fidele Ntie-Kang of the Chemical and Bioactive Information Center, Department of Chemistry, University of Buea, Cameroon is acknowledged for his help with computational tools. Junior Researcher Grant awarded to Akachukwu Ibezim by The African-German Network of Excellence in Science (AGNES) is gratefully acknowledged.

Supporting information

CCDC-1860214 contains the supplementary crystallographic data for this paper. These data can be obtained free of charge via www.ccdc.cam.ac.uk/data_request/cif, or by e-mailing data_request@ccdc.cam.ac.uk, or by contacting The Cambridge Crystallographic Data Centre, 12 Union Road, Cambridge CB2 1EZ, UK; fax: +44(0)1223-336033.

Disclosure statement

Conflict of interests: The authors declare that they have no conflict of interest.

Author contributions: All authors contributed equally to this work.

Ethical approval: All ethical guidelines have been adhered.

Sample availability: Samples of the compound is available from the authors.

ORCID

Ifeyinwa Stella Ozochukwu

 <https://orcid.org/0000-0001-8148-2379>

Obinna Chibueze Okpareke

 <https://orcid.org/0000-0003-0815-8198>

David Chukwuma Izuogu

 <https://orcid.org/0000-0002-1497-2308>

Akachukwu Ibezim

 <https://orcid.org/0000-0003-1620-5716>

Oguejiofo Theophilus Ujam

 <https://orcid.org/0000-0002-5628-209X>

Jonnie Niyi Asegbeloyin

 <https://orcid.org/0000-0002-5710-7613>

References

- [1]. Fonkui, T. Y.; Ikhile, M. I.; Ndinteh, D. T.; Njobeh, P. B. *Trop. J. Pharm. Res.* **2019**, *17* (12), 2507–2518.
- [2]. Hegazy, W. H. *Eur. J. Chem.* **2014**, *5* (3), 415–418.
- [3]. Kumar, H.; Chaudhary, R. P. *Der Chemica Sinica* **2010**, *1* (2), 55–56.
- [4]. Asegbeloyin, J. N.; Ujam, O. T.; Okafor, E. C.; Babahan, I.; Coban, E. P.; Ozmen, A.; Biyik, H. *Bioinorg. Chem. Appl.* **2014**, *2014*, 718175.
- [5]. Asegbeloyin, J. N.; Izuogu, D. C.; Oyeka, E. E.; Okpareke, O. C.; Ibezim, A. J. *Mol. Struct.* **2019**, *1175*, 219–229.
- [6]. Arafath, M. A.; Adam, F.; Razali, M. R.; Ahmed Hassan, L. E.; Ahamed, M. B. K.; Majid, A. M. S. A. *J. Mol. Struct.* **2017**, *1130*, 791–798.
- [7]. Hussein, T. I.; Ahmed, M. A.; Arbab, I. A.; Ibrahim, A. S.; Al-Bratty, M.; Alhazmi, H. A.; Najmi, A. *Eur. J. Chem.* **2020**, *11* (1), 15–20.

- [8]. Andiappan, K.; Sanmugam, A.; Deivanayagam, E.; Karuppasamy, K.; Kim, H.-S.; Vikraman, D. *Sci. Rep.* **2018**, *8* (1), 3054-3065. <https://doi.org/10.1038/s41598-018-21366-1> (accessed Apr 8, 2021).
- [9]. Malladi, S.; Isloor, A. M.; Isloor, S.; Akhila, D. S.; Fun, H.-K. *Arab. J. Chem.* **2013**, *6* (3), 335-340.
- [10]. El-Shekeil, A. G.; Abubakar, A. O.; Al-Aghbari, S. A.; Nassar, M. Y. *Eur. J. Chem.* **2014**, *5* (3), 410-414.
- [11]. Abd-Elzaher, M. M.; Labib, A. A.; Mousa, H. A.; Moustafa, S. A.; Ali, M. M.; El-Rashedy, A. A. *Beni-Suef Univ. J. Basic Appl. Sci.* **2016**, *5* (1), 85-96.
- [12]. Nagesh, G. Y.; Mahendra Raj, K.; Mruthyunjayaswamy, B. H. M. *J. Mol. Struct.* **2015**, *1079*, 423-432.
- [13]. Bhat, M. A.; Al-Omar, M. A. *Acta Pol. Pharm.* **2011**, *68* (3), 375-380.
- [14]. Nithinchandra; Kalluraya, B.; Aamir, S.; Shabaraya, A. R. *Eur. J. Med. Chem.* **2012**, *54*, 597-604.
- [15]. Ashutosh, K. Medicinal Chemistry; New Age International Ltd.: New Delhi, India, 2007; pp. 794.
- [16]. Gibbs, J. B. *Science* **2000**, *287* (5460), 1969-1973.
- [17]. WHO Media Centre. Cancer <https://www.who.int/en/news-room/fact-sheets/detail/cancer> (accessed Apr 8, 2021).
- [18]. Globocan Fact Stats, <https://gco.iarc.fr/> (accessed Apr 8, 2021).
- [19]. Giaccone, G. *Drugs* **2000**, *59* (Supplement 4), 9-17.
- [20]. Fuertes, M. A.; Alonso, C.; Pérez, J. M. *Chem. Rev.* **2003**, *103* (3), 645-662.
- [21]. Gasser, G.; Ott, I.; Metzler-Nolte, N. *J. Med. Chem.* **2011**, *54* (1), 3-25.
- [22]. APEX-2. Bruker-Nonius AXS. 2008, Bruker AXS, Madison, Wisconsin, USA.
- [23]. Sheldrick, G. M. *Acta Crystallogr. A* **2008**, *64* (1), 112-122.
- [24]. Turner, M. J.; McKinnon, J. J.; Wolff, S. K.; Grimwood, D. J. Spackman, P. R.; Jayatilaka, D.; Spackman, M. A. *CrystalExplorer17*. The University of Western Australia, 2017.
- [25]. Spackman, M. A.; McKinnon, J. J. *CrystEngComm* **2002**, *4* (66), 378-392.
- [26]. Tan, S. L.; Jotani, M. M.; Tiekink, E. R. T. *Acta Crystallogr. E Crystallogr. Commun.* **2019**, *75* (Pt 3), 308-318.
- [27]. Molecular Operating Environment (MOE), 2010.01; Chemical Computing Group ULC, 1010 Sherbooke St. West, Suite #910, Montreal, QC, Canada, H3A 2R7, 2010.
- [28]. Ntie-Kang, F.; Nwodo, J. N.; Ibezim, A.; Simoben, C. V.; Karaman, B.; Ngwa, V. F.; Sippl, W.; Adikwu, M. U.; Mbaze, L. M. *J. Chem. Inf. Model.* **2014**, *54* (9), 2433-2450.
- [29]. Govindaraj, V.; Ramanathan, S. *Turk. J. Chem.* **2014**, *38*, 521-530.
- [30]. Ejidike, I. P.; Ajibade, P. A. *Bioinorg. Chem. Appl.* **2015**, *2015*, 890734.
- [31]. Yusnita, J.; Puvaneswary, S.; Mohd. Ali, H.; Robinson, W. T.; Kwai-Lin, T. *Polyhedron* **2009**, *28* (14), 3050-3054.
- [32]. Tan, S. L.; Tiekink, E. R. T. *Acta Crystallogr. E Crystallogr. Commun.* **2020**, *76* (Pt 1), 102-110.
- [33]. Izuogu, D. C.; Asegbeloyin, J. N.; Jotani, M. M.; Tiekink, E. R. T. *Acta Crystallogr. E Crystallogr. Commun.* **2020**, *76* (Pt 5), 697-702.
- [34]. Mackenzie, C. F.; Spackman, P. R.; Jayatilaka, D.; Spackman, M. A. *IUCr* **2017**, *4* (Pt 5), 575-587.
- [35]. Lipinski, C. A. *J. Pharmacol. Toxicol. Methods* **2000**, *44* (1), 235-249.
- [36]. Hast, M. A.; Fletcher, S.; Cummings, C. G.; Pusateri, E. E.; Blaskovich, M. A.; Rivas, K.; Gelb, M. H.; Van Voorhis, W. C.; Sebt, S. M.; Hamilton, A. D.; Beese, L. S. *Chem. Biol.* **2009**, *16* (2), 181-192.
- [37]. Shima, F.; Ijiri, Y.; Muraoka, S.; Liao, J.; Ye, M.; Araki, M.; Matsumoto, K.; Yamamoto, N.; Sugimoto, T.; Yoshikawa, Y.; Kumasaka, T.; Yamamoto, M.; Tamura, A.; Kataoka, T. *J. Biol. Chem.* **2010**, *285* (29), 22696-22705.



Copyright © 2021 by Authors. This work is published and licensed by Atlanta Publishing House LLC, Atlanta, GA, USA. The full terms of this license are available at <http://www.eurjchem.com/index.php/eurjchem/pages/view/terms> and incorporate the Creative Commons Attribution-Non Commercial (CC BY NC) (International, v4.0) License (<http://creativecommons.org/licenses/by-nc/4.0>). By accessing the work, you hereby accept the Terms. This is an open access article distributed under the terms and conditions of the CC BY NC License, which permits unrestricted non-commercial use, distribution, and reproduction in any medium, provided the original work is properly cited without any further permission from Atlanta Publishing House LLC (European Journal of Chemistry). No use, distribution or reproduction is permitted which does not comply with these terms. Permissions for commercial use of this work beyond the scope of the License (<http://www.eurjchem.com/index.php/eurjchem/pages/view/terms>) are administered by Atlanta Publishing House LLC (European Journal of Chemistry).